Journal of Materials Processing Tech. 302 (2022) 117470

Contents lists available at ScienceDirect

Journal of Materials Processing Tech.

journal homepage: www.elsevier.com/locate/jmatprotec

Direct-Ink-writing of liquid metal-graphene-based polymer composites: Composition-processing-property relationships

Ruchira Tandel, B. Arda Gozen *

Washington State University, School of Mechanical and Materials Engineering, Pullman, WA, 99164, United States

ARTICLE INFO

Associate Editor: Jian Cao

Keywords:
Liquid metals
Direct-ink-writing
Electrical conductivity
Viscoelasticity

ABSTRACT

This paper presents a study of the solvent-based precursors (inks) derived from composites of polyethylene oxide, graphene flakes and micro-scale spherical Eutectic Gallium Indium (EGaIn) fillers and their processing through direct-ink-writing (DIW). The presented studies focus on the influence of EGaIn fillers on ink rheology, DIW process mechanisms as well as electrical conductivity of the printed structures. The results show that EGaIn fillers vary the ink rheology towards a more elastic behavior with lower extensional viscosity. This leads to ink filaments capable of withstanding large extensional strains during DIW, forming continuous prints even when printing speed is higher than ink flow speed, and producing features with line width smaller than the nozzle diameter. Electrical conductivity of the prints reduces with increasing strain due to the deformation of the liquid EGaIn fillers along the printing direction. These findings can be utilized to control the DIW process and the properties of the conductive polymer composites.

1. Introduction

Polymer composites (PCs) synergistically combine the desired properties of polymers (e.g. mechanical toughness, dielectric loss) and filler particles (e.g. electrical and thermal conductivity) to yield unique bulk properties that cannot be achieved by other material systems. PCs have been utilized in a number of technologies including tissue engineering (Dababneh and Ozbolat, 2014), energy storage (Wei et al., 2017), wearable and conformable electronics (Muth et al., 2014), and biochemical sensing (Nesaei et al., 2018). These unique properties are strong functions of the filler particle properties and their organization within the composites, which is primarily driven by the methods used to process these materials. The processing of such complex systems is also highly dependent upon the rheological properties of the composite constituents, which renders the PC development and manufacturing a challenging task. As such, there is an emerging demand for research focusing on new material systems and the unique processing methods to unlock the new properties and functionalities that can be achieved using PCs.

Among the most common fillers used in PCs are carbon-based, such as carbon nanotubes (Chatterjee and Krishnamoorti, 2013), carbon black (Donnet and Vidal, 1986), graphene (Sun et al., 2013b), and graphite (Seah and Pumera, 2011) for thermal and electrical conductivity improvement. Other examples include ceramics (Li et al., 2015) and clay nanocomposites such as silica organoclay (Zhao et al., 2005) or metallic fillers (Skylar-Scott et al., 2016). A new type of filler that have recently drawn attention are the ones derived from eutectic alloys that have melting points below room temperature including Eutectic Gallium-Indium (EGaIn) or Galinstan. These liquid metal particles are encapsulated by their oxide skin which render them soft and deformable unlike conventional rigid fillers. Addition of EGaIn fillers to PCs has been shown to improve their toughness and tear resistance significantly (Kazem et al., 2018) by increasing the energy dissipation due to the deformability of liquid metal inclusions under loading. It has also been demonstrated that the addition of EGaIn enhances thermal and electrical conductivity of elastomeric parts (Bartlett et al., 2017; Boley et al., 2014; Zhu et al., 2013). Interestingly, the presence of the nanometric oxide skin prevents these particles from forming conductive pathways even above their percolation thresholds (Boley et al., 2015). Accordingly, unlike many metal nanoparticle additives, PCs with EGaIn additives are not inherently electrically conductive, unless they go through a mechanical sintering process to rupture the particles and form conductive pathways (Neumann et al., 2020). EGaIn fillers can still make contributions to composites' electrical conductivity when used in conjunction with other rigid conductive fillers specifically acting as stretchable anchors between the rigid particles thus realizing

* Corresponding author.
E-mail address: arda.gozen@wsu.edu (B.A. Gozen).

https://doi.org/10.1016/j.jmatprotec.2021.117470
Received 9 September 2021; Received in revised form 7 December 2021; Accepted 12 December 2021
Available online 13 December 2021

conductivity under deformation (Guo et al., 2020; Wang et al., 2018). In addition to electrical conductivity, such multi-filler systems can be utilized to achieve desirable thermal (Sargolzaeiaval et al., 2019; Tutika et al., 2018) and piezoelectric (Yun et al., 2020) properties. These capabilities can enable functional material systems that can be utilized in emerging flexible electronics, soft robotics and wearable device applications where such properties under mechanical strains are critically needed.

Primary manufacturing challenge for the PC systems in general is the need for high resolution control of the filler distribution and morphology within the polymer matrix which impacts the functional properties of the final products. This challenge is more prevalent for highly complex PCs including multiple fillers such as EGaIn fillers along with rigid counterparts. Emerging additive manufacturing methods such as micro-extrusion-based printing or direct-ink-writing (DIW) carry a potential to address this challenge since it can control material deposition within layers as small as tens of microns in thickness. Studies on DIW with carbon fiber, carbon nanotube or graphene-based PNs showed that the nanofillers tend to align along the flow direction under the influence of shear and extensional stresses (Jakus et al., 2015; Wang and Smith, 2018), leading to increased bulk conductivity. Flow of such inks and the associated stresses are strong functions of their shear and extensional rheology which in turn is heavily influenced by the filler type and concentration (Majesté, 2016). Recent studies on PC inks including liquid metal fillers demonstrated the unique properties of such material systems. Specifically, unlike rigid fillers, EGaIn fillers reduced shear and extensional viscosity of the inks while increasing their relaxation times substantially (Nesaei et al., 2019). When combined with other rigid fillers, liquid metal particles and the unique rheological properties they induce can enable increased levels of control over the ink flow, resultant filler morphology and final part properties during the DIW process. To realize such capabilities, in-depth studies on the rheology of PCs including liquid metal and rigid conductive fillers, and their processing through the DIW approach is needed.

In this paper, we present an in-depth study on one of such PC systems consisting of poly(ethylene oxide) (PEO) as the polymer matrix and, EGaIn microparticles along with graphene flakes as fillers. We characterize shear and extensional rheology of the inks of various compositions derived from this system, study the flow and deposition of such inks during the DIW process along with the electrical conductivity of the printed structures. Our particular aim is to answer two key questions: (1) how the unique rheological properties inducing by EGaIn fillers in a graphene-based PC ink influence the printability and feature resolution particularly for the under-extrusion regime where the ink flow speed is less than the printing speed, (2) how do EGaIn fillers contribute to the electrical conductivity of these composites and how does this contribution vary with DIW process parameters. These studies will reveal the functional value of the liquid metal fillers when used in conjunction with other fillers, specifically regarding processability and electrical conductivity. In the following section, we introduce various ink compositions studied and their preparation, rheological characterization methods, details on the DIW experiments and characterization of the printed structures. Results of the rheological characterization and DIW experiments are then presented along with key discussions towards answering the aforementioned questions.

2. Materials and methods

2.1. Materials and ink preparation

2.1.1. Materials

Composite inks studied in this work comprised of Graphene Nanopowder (Grade: AO-4: 60 nm, purchased from Graphene Supermarket) and EGaIn (75 % w/w Gallium from Rotometals, 25 % w/w Indium from Unique Metals) microparticles as conductive fillers inside a Polyethylene Oxide (PEO) matrix. All inks were prepared in a solution form with Acetonitrile (anhydrous, 99.8 %, from Sigma Aldrich) as solvent at a constant volumetric solid (filler and matrix) concentration of 30 %. The overall compositions of the inks studied are summarized in Table 1. Three ink compositions that incorporate both Graphene and EGaIn fillers were used, where total filler concentration was kept at 5% by volume. The main motivation behind limiting the total filler concentration at 5% by volume, lies with our interest in the under-extrusion regime of the DIW process where the ink flow speed is less than the printing speed as detailed in Section 3.2.3. Inks with higher filler concentration than 5% exhibited both high shear viscosity and low extensional relaxation time such that continuous line formation under the specific process regime and the associated large extensional strains, was difficult.

Three distinct levels of EGaIn fillers volumetric concentration were used at 1, 2 and 2.5 %. Additionally, two control inks that include the same amount of graphene fillers while replacing the EGaIn volume with the PEO binder. These inks are marked with an asterisk in Table 1. The control inks were used to objectively study the influence of EGaIn fillers on the ink rheology, 3D printing behavior and electrical conductivity. A blend of two different molecular weight Polyethylene Oxide (PEO) (LWM: 10^5 g/mol and HMW: 5×10^6 g/mol, purchased from Sigma Aldrich) were used as a binder to form a polymer matrix at a weight ratio of 100:3. This approach allowed us to tune the viscoelastic behavior of the inks through relative composition of the two molecular weight polymers as described in our earlier studies (Nesaei et al., 2019, 2017). Inks consisting only of EGaIn fillers did not yield structures exhibiting electrical conductivity, which is expected from the earlier findings in the literature regarding the inability of EGaIn particles to form conductive pathways (Boley et al., 2015). Given that the influence of composition and DIW-based processing on the electrical conductivity is a critical part of our analyses, we did not include any inks including only EGaIn fillers.

2.1.2. Ink preparation

EGaIn was prepared by mixing molten gallium (75 % weight) and indium (25 % weight). Both metals were melted around 170 °C, hand mixed in a crucible for 25−35 min on a heated plate (Fisher Scientific, Isotemp), followed by air cooling to the room temperature. EGaIn was sonicated in Acetonitrile using a sonicator probe (YUCHENGTECH Ultrasonic Homogenizer Sonicator Processor Mixer, 600 W, 20−500 ml) for about 90−120 min. The LMW PEO and Graphene nanoflakes were gradually added into the EGaIn dispersion while continuously mixing it using a mechanical mixer (Cole-Parmer Compact Digital Mixer System) at a speed of 200 RPM. The dispersion is mixed for an additional 30 min at a speed of 350 RPM to ensure complete dissolution of PEO and homogenization of the inks. Next, HMW PEO was steadily added to the solution. The mixing speed was reduced to 200RPM to mitigate rod climbing (or Weissenberg) (Nimmakayala and Raju, 2015) effects arising due to the increase in ink viscoelasticity caused by HMW PEO addition. Following the continuous mixing for another 30 min, the ink was transferred to 3cc syringes for further characterization and 3D printing experiments. The inks were stored inside sealed syringes at room temperature on a tube roller mixer to minimize settling of constituents. Pictures of a representative ink, EG2.5, stored in syringes is

Table 1
Compositions of the inks that were studied. Control inks are marked with an asterisk.

	Volumetric Percentage			
	EGaIn	Graphene	PEO	Acetonitrile
EG2.5	2.5	2.5	25	70
E2G3	2	3	25	70
E1G4	1	4	25	70
G5	0	5	25	70
G2.5*	0	2.5	27.5	70
G4*	0	4	26	70

given in Fig. S2. The syringes were mixed in a centrifugal mixer (Thinky Mixer, Non-Vacuum, AR-100, 140 g) for 40 s before every experiment at a speed of 2000 RPM.

2.2. Rheological characterization

Rheological characterization of the inks was performed using a rotational rheometer (TA Instruments ARES-G2) also capable of performing capillary breakup experiments for extensional rheometry. This system controls the shear and extensional strain rate precisely while measuring the torque and normal force applied between two plates between which the inks are introduced. Through these measurement shear stress and normal stress acting the on the inks are determined to characterize their shear and extensional rheology. The specific characterization experiments are detailed below:

2.2.1. Shear rheology

Shear rheology was characterized using cone and plate setup (50 mm diameter with a cone angle of 0.0196 rad and a gap of 0.0477 mm between the plates) and a flow ramp experiment where the strain rate was logarithmically increased from 0.1 s^{-1} to 100 s^{-1} to characterize non-Newtonian viscosity-shear rate behavior of the inks. For each ink composition one experiment using 0.64 mL ink sample was used. During the experiments, the ink between the plates was surrounded by mineral oil to avoid solvent evaporation. Oscillatory amplitude sweep tests were employed before running the flow ramp test to ensure that the transient material behavior is suppressed during the strain rate increase.

2.2.2. Extensional rheology

Extensional rheometry through capillary break up experiments were performed using 0.1 mL of ink squeezed between 25 mm diameter parallel plates with an initial gap of 1 mm. The plates were moved away from each other by 12 mm at constant Hencky strain rates of 0.5,1,1.5 and 2 s^{-1} obtained through exponentially increasing velocity (Spiegelberg et al., 1996). As such, a total of five samples of 0.1 mL ink were tested for each composition, with each sample being tested with different strain rates. The force along the motion direction was measured as a function of time while the thinning of the ink filament was observed through a microscope camera as shown in Fig. 1(a). At the end of the stretching motion, the filament relaxation was further observed for an additional 20 s. Following the tests, mid-filament diameters were measured through image processing of the process videos using a custom MATLAB code (Fig. 1(b)). For the first part of the experiments where the top plate is in motion (stretching phase), the force vs filament diameter data was used to determine the transient extensional viscosity of the inks as a function of the Hencky strain. In the second phase where the top plate is stationary (relaxation phase), the time variation of the filament diameter is used to determine the relaxation time of various inks. While processing the relaxation data, the values extracted from the 5 tests per composition were averaged as since no clear influence of the extension rate on the material behavior during the relaxation phase was observed. This is consistent with the literature for similar materials(Nesaei et al., 2019; Spiegelberg et al., 1996).

2.3. 3D printing

2.3.1. 3D printer setup

3D printing was performed using a custom direct ink writing system as shown in Fig. 2. This system features a 3-axis motion system (Aerotech ANT180-ANT130 stages), which translates the build plate in three dimensions with sub-micron accuracy. A pneumatic time-pressure approach was used to dispense the inks during the printing process. To that end, a digital dispensing valve (Nordson UltimusPlus 1) is used to apply controlled air pressures at the back of the piston of the syringe carrying the ink with 14 kPa precision. The pressurized air source to this dispenser was regulated at 552 kPa. For experiments that require higher

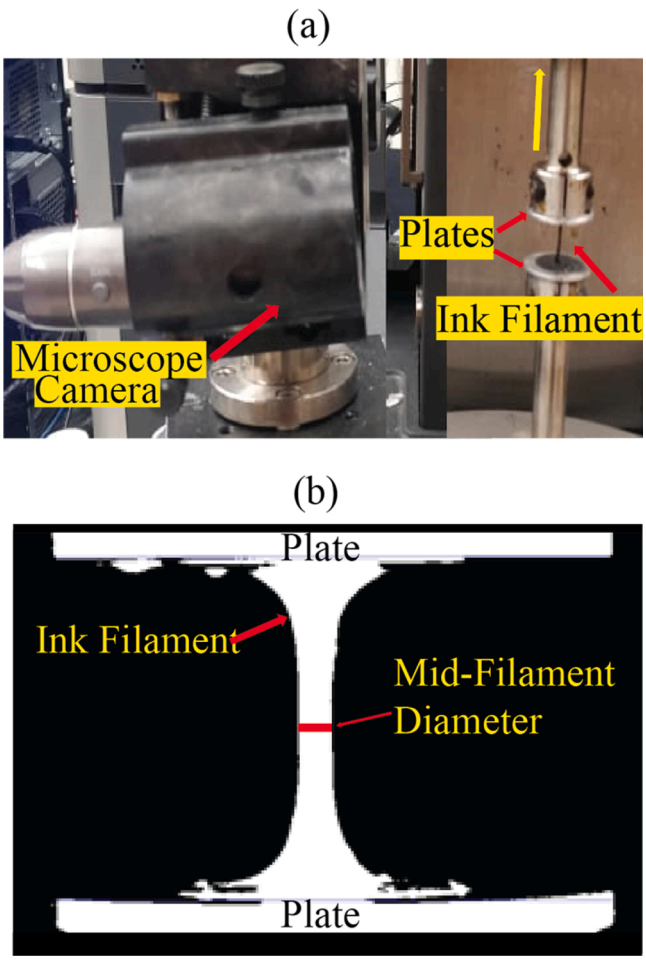

Fig. 1. a) Extensional Rheometry setup. (b) Image processing of ink filament during extensional rheology.

dispensing pressures, high pressure dispensing tool (Nordson HP5cc) was used behind the syringe piston. To measure and precisely control nozzle-standoff distance (the distance between the nozzle and the substrate during the printing process), this system features two metrology tools: a piezoelectric force sensor (PCB Piezotronics 484B06) and a laser displacement sensor (Keyence LT9031 M) (See section S1.1 in the supporting information for the detailed procedure to control the nozzle standoff distance). A custom LabView interface is used to execute the automated printing and metrology tasks by commanding the motion stages, digital dispenser, the force sensor, and the laser displacement sensor. A microscope camera (Sentech STC MCCM200U3V) was used to visually monitor the printing process.

2.3.2. 3D printing experiments

The 3D printing of the composite inks was explored through experiments where linear structures were printed from each ink using various sets of process parameters including flow rate, printing speed and nozzle-standoff distance. All experiments were performed using nozzles with 200 μm inner diameter (Nordson 7,018,462) and glass substrates. The nominal levels of flow rate, printing speed and stand-off distance that were used in the experimentation is presented in Table 2. Among these parameters the flow rates and print speeds were specifically selected to explore the under-extrusion regime of the direct-ink-writing process, where the average speed of the ink flow at the nozzle exit is less than the printing speed as demonstrated in Fig. 3. Under this regime, ink filaments experience a finite "stretch" (Yuk and Zhao, 2018) after they leave the nozzle and before they are deposited onto the substrate as shown in Fig. 3. The specific values of flow rates/speeds were selected

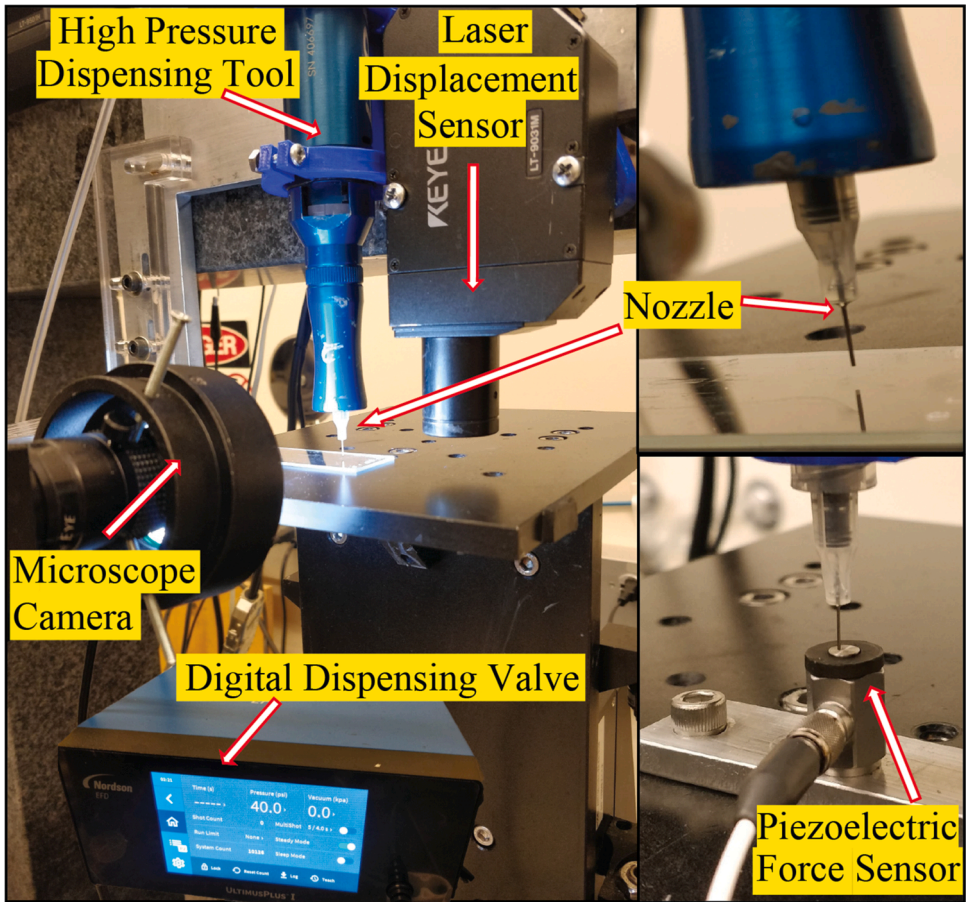

Fig. 2. DIW setup.

Table 2
DIW process parameters.

Parameters	Units			
Print Speed	mm/s	7	15	25
Standoff Distance	microns	100	200	300
Flow Rates (Average Ink Flow Speed)	m^3/s (mm/s)	3×10^{-11}(0.95)	6×10^{-11}(1.91)	9×10^{-11}(2.87)

through experimental observation such that a moderate dispensing pressure range between 250–950 kPa would be required to achieve these rates for the materials of interest. We observed that higher pressures lead to ink back flow near the syringe piston whereas lower pressures/flow rates are difficult to achieve in a consistent manner. Finally, the standoff distance values were selected as the 0.5, 1 and 1.5 times the nozzle diameter (200 μm). This is motivated by some of the earlier studies on the DIW process where the ratio between the standoff distance the nozzle diameter is studied (Boley et al., 2014; Yuk and Zhao, 2018). For each parameter set, three straight lines of 70 mm length were printed consecutively.

To achieve the desired flow rates using a time-pressure system, where the dispensing pressure, rather than the flow rate is controlled, additional experimentation was necessary. Specifically, to determine the pressures required to achieve desired flow rate levels for a given material, inks were dispensed at various pressures for 120 s, were collected in sealed containers and weighed. The dispensed ink volume flow rate was then calculated using known density of the inks and the dispensing

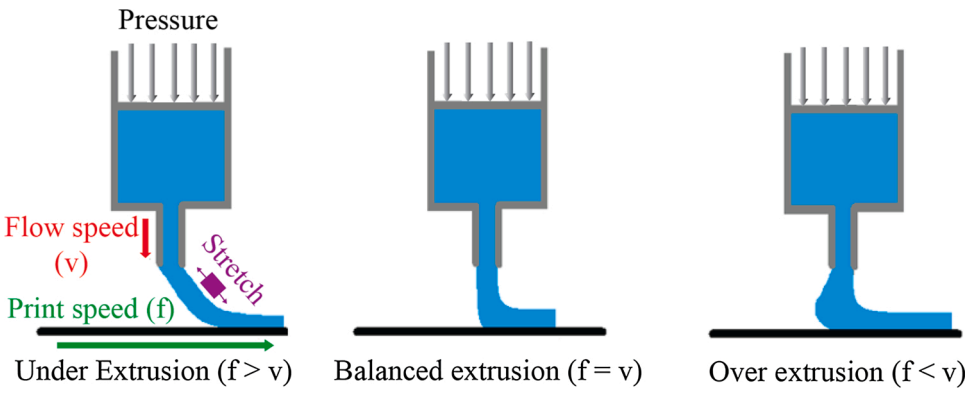

Fig. 3. Various extrusion regimes in DIW.

duration. The three pressure levels producing the three desired flow rate levels were then used during the printing experimentation for the corresponding material. Through this approach a flow rate accuracy of 2×10^{-11} m^3/s was achieved. The exact flow rates (with deviations around the target values within the reported accuracy) observed in the experiments were recorded and used during the analyses of the experimental data.

2.4. Characterization of the 3D printed structures

2.4.1. Geometric and morphological characterization

To quantitatively characterize the geometry of the prints Zygo NewView 6300 3D profilometer with a 50x scan lens was used. Geometric features such as width, height and volume were measured to calculate the electrical conductivity from resistance measurements. Scanning Electron Microscope (SEM, FEI Quanta 200 F, ThermoFisher, Courtesy of WSU FMIC) with a 1000x zoom, 11 mm working distance and 500 V beam power was used to scan the printed lines to analyze the morphology of the composite constituents in the printed structures.

2.4.2. Electrical conductivity characterization

Kelvin-probe method was used to measure the DC resistance of the printed lines using an LCR meter (BK Precision Model 894, 500 kHz), to characterize their electrical conductivity. For each printing condition, the resistance of three repetition lines were measured simultaneously in a parallel fashion. Droplets of liquid EGaIn were used as conformable and low resistance electrodes (Chiechi et al., 2008) during these measurements to establish robust electrical contact between the measurement probes and the printed lines while avoiding damage to the lines. To this end, EGaIn droplets, large enough to cover all three lines, were dispensed at several locations along the length of the lines. Images of the lines with EGaIn contacts are included in Figure S3 of the supporting information. To eliminate the effect of contract resistance, line-transmission approach (Harrison, 1989) was used by measuring the resistance across various lengths along the lines. Here, the resistance is represented as a linear function of the line length as follows:

$$R = \frac{1}{\sigma A} L + R_c \tag{1}$$

Where A is the average cross-sectional areas of the lines, L is the line length, determined through optical profilometry, σ is the conductivity of the lines and R_c is the total contact resistance. As such, the conductivity is calculated linear regression of the obtained R-L curves and determination of the reciprocal of their slopes and dividing them by A. The detailed experimental procedure followed to perform Kelvin-Probe and Line Transmission measurements using EGaIn contacts is explained in the Supporting Information Section S1.2.

3. Results and discussions

3.1. Ink rheology

3.1.1. Shear rheology

Resulting shear viscosity and stress vs strain rate data corresponding to a representative ink, EG2.5, presented in Fig. 4(a). The data corresponding to the rest of the inks is provided in Fig S4. Generally, inks exhibited a distinct zero-shear rate viscosity and no distinct yield stress, combined with a shear thinning nature. Fig. 4(b) highlights the variation of zero shear rate viscosity corresponding to different inks as obtained through fitting a Carreau-Yasuda viscosity model to this experimental data. It is evident from this data that higher graphene content leads to higher zero shear rate viscosity. EG2.5 and E1G4, compared to the control inks G2.5 and G4, did not exhibit a significantly different shear viscosity, with a slight reduction for the ink that has the higher EGaIn content, EG2.5 and a slight increase for E1G4.

3.1.2. Extensional rheology

Resulting transient extensional viscosity vs Hencky strain data corresponding to a representative ink, EG2.5, presented in Fig. 4(c). The data corresponding to the rest of the inks is provided in Fig S5. All the inks exhibited a strain hardening behavior during the stretching phase of the capillary breakup experiments, with a near constant (plateau) viscosity at low strains which increases rapidly at high strains. Fig. 4(d) shows the variation of the plateau extensional viscosity for all inks. Two

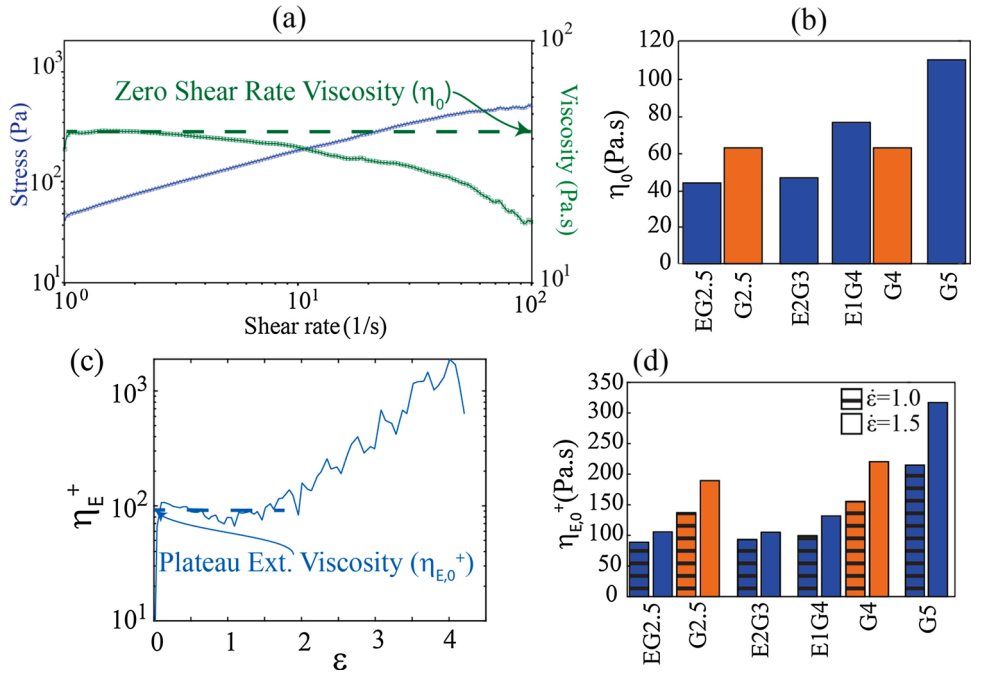

Fig. 4. Results of the rheological characterization (a) Sample flow ramp test result for EG2.5, (b) Zero-shear rate viscosities of different inks, (c) Transient extensional viscosity profile of EG2.5, (d) Plateau extensional viscosities of different inks.

data points provided for each ink represents the results obtained at two different strain rates. These results indicate that presence of the EGaIn fillers leads to a discernible decrease in extensional viscosity. Furthermore, EGaIn fillers reduce the strain-rate dependent hardening of the inks: The rate dependent increase of the extensional viscosity is higher for E1G4 compared to EG2.5, and both inks exhibit a substantially lower rate-dependent viscosity increase when compared to the control inks.

Fig. 5(a) shows the relaxation profiles (normalized filament diameter vs. time during the relaxation phase of the extensional rheometry tests) for two representative inks EG2.5 and E1G4. This data was utilized to determine the effective relaxation time for each ink through Oldroyd-B viscoelastic model fitting. Specifically, each relaxation profile was least square fitted with a three-mode Oldroyd-B model which predicts the diameter variation during relaxation as follows (Anna and McKinley, 2001);

$$\frac{D(t)}{D(0)}\left(\sum_{i=1}^{3} K_i D(0)\exp(-t/\lambda_i)\right)^{1/3} \quad (2)$$

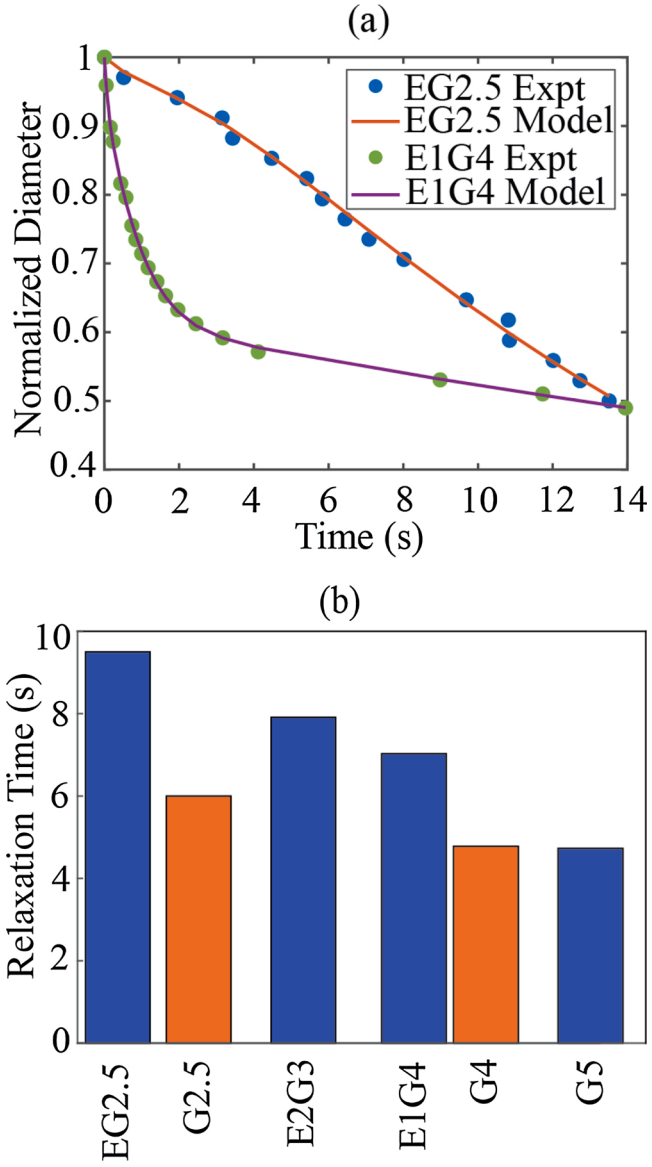

Fig. 5. Characterization of the relaxation behavior of various inks; (a) Temporal relaxation profile of two sample inks along with the 3-mode Oldroyd-B model fits, (b) Relaxation times of different inks.

Where K_i is a material constant that is a function of elastic modulus corresponding to a given mode and surface tension and, λ_i is the relaxation time, corresponding to a given mode, and D(t) is the filament diameter measured at time t, with t = 0 corresponding to the instant where the top plate stops moving during the experiments. The representative model fits are shown in Fig. 5(a). The data corresponding to the rest of the inks is provided in Fig S6. Following this fitting, the highest relaxation time across the three modes were selected as the effective relaxation time for the material (Anna and McKinley, 2001). The average relaxation times were accordingly calculated for each material across different experiments and shown in Fig. 5(b). It is evident from this figure that inclusion of EGaIn fillers yield a distinct increase in relaxation time of the inks. This result is consistent with the earlier findings regarding the PEO-EGaIn composites (without graphene) (Nesaei et al., 2019) and can be explained by the elasticity of the oxide covered liquid EGaIn particles (Lear et al., 2017).

3.2. 3D printing

Results of the experiments outlined in 2.3.2 were categorized to four categories as function of the general morphology of the printed lines as illustrated in Fig. 6(a). Here, continuous (C) prints refer to lines that were generated with homogenous width throughout their lengths, marginally continuous (MC) lines, despite being connected throughout. Show local reductions in width at several locations, “blobby” (B) lines show a periodic pattern consisting of a large ink deposit followed by a thin line, discontinuous (D) lines exhibit disconnections of various lengths. Videos of the printing processes leading to each of the four types of lines is provided as a part of the supporting information. During the printing of C-type lines, the ink forms a steady filament that is stretched under extensional flow (since the under-extrusion regime is studied) between the nozzle and the substrate as it is being deposited. B-type lines are observed when the ink flowing out of the nozzle forms a growing bubble at the nozzle exit rather than exhibiting extensional flow between the nozzle and the substrate as observed in the C-type lines. When the height of the bubble reaches the standoff distance, it is deposited on the substrate, forming a transient filament between the nozzle and the substrate, which thins down as a new droplet forms but does not fail until the new droplet gets deposited. MC-types lines exhibit rather sporadic transitions between the C and B type lines, likely due to small variations in the ink composition that is flowing through the nozzles. In the case of the D-type lines, the filaments forming between the nozzle and the substrate fail leading to a disconnected pattern. To understand how the ink rheology and the printing parameters influence the formation of these different results, we considered two non-dimensional parameters: $\varepsilon = 4Q/\pi D^2 f$ and $Ec = \sigma\lambda/\eta_0 H$. Here, the printing strain (ε) is the strain experienced by the printed filament as it flows between the nozzle and the substrate. It is simply the ratio between the average speed of the ink exiting the nozzle and the printing speed (i.e. the speed of the substrate), incorporating the ink flow rate Q, nozzle diameter D and printing speed f. The Elastocapillary number (Ec) is a commonly used non-dimensional parameter that quantifies the interplay between the capillary-elastic and viscous effects in a given material-process pair (Clasen et al., 2012; Mckinley, 2005). Here σ is the surface tension, λ is the relaxation time and η_0 is the zero-shear rate viscosity of the inks and H is the stand-off distance during printing. All these parameters other than surface tension is either characterized through the results presented in Section 3.1 or prescribed during the experiments, except for the surface tension. For viscoelastic materials such as the inks considered in this work, the free surface behavior is heavily dominated by elastic and viscous effects rather than surface tension (Rošic et al., 2012) which renders the use of conventional experimental techniques to measure surface tension, such as pendant drop, impossible. In the limited number of studies in the literature which focus on polymer solutions or composite inks with low solid concentration, it has been shown that variation in polymer and particle concentration causes a deviation from the

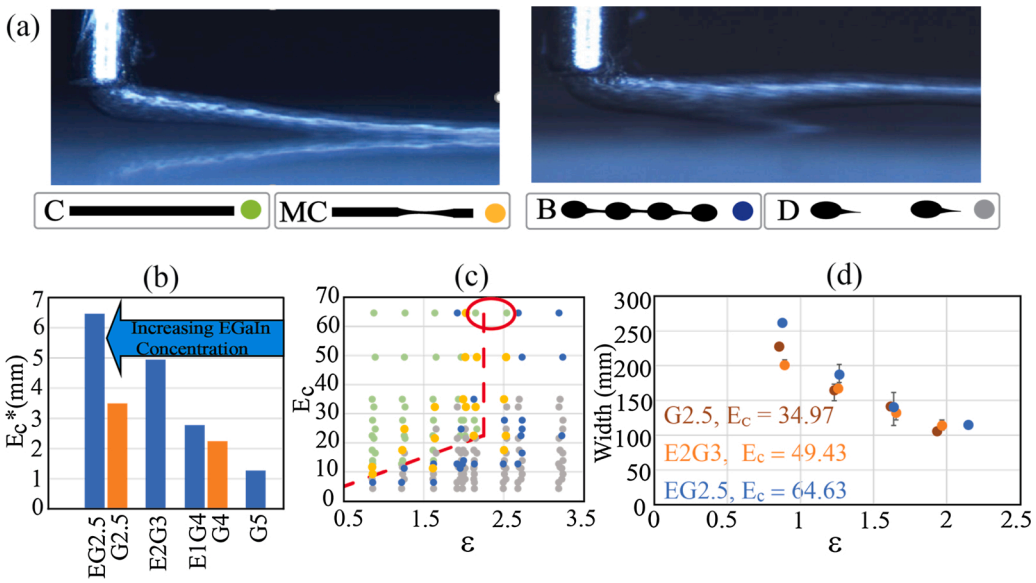

Fig. 6. Results of the printing experiments; (a) Morphological categorization of the printed lines, (b) Ec* values for each ink, (c) Results of all printing experiments on the Ec-e plane. Each experiment is represented with a dot, the color of which is determined by the categorization given above, (d) Strain dependent variation of linewidth for three materials.

solvent surface tension generally within 1–1.5 % per 1% increase in solid concentration (Elliott et al., 2012; Lipatov and Feinerman, 1971). Since the main purpose of this analysis is to compare the Ec values across the inks of interest, we consider the fact that the solute concentration for all the inks is the same at 30 % and the particle composition varies only within 2.5 % volumetrically. We accordingly implemented constant surface tension value across the inks, equal to the surface tension of solvent Acetonitrile (0.02929 N/m).

The portion of the Elastocapillary number that represents material rheology is given by $Ec^* = HEc$, which we refer to as the Elastocapillary height of a given ink. This quantity was calculated for each ink using the relaxation time and zero-shear rate characteristics detailed in Section 3.1. Fig. 6(b) illustrates that the Ec^* increases with the increasing EGaIn and decreasing Graphene content in the inks, due to the increased relaxation time and reduced shear viscosity. Comparison of the Ec^* values between the EG2.5 and G2.5 as well E1G4 and G4 inks demonstrate the distinct influence of EGaIn fillers on the elastocapillarity of the inks.

Fig. 6(c) presents the classification of all printed lines mapped in the ε -Ec plane. Here, each experiment is denoted with a single circle, color of which depicts the classification of the result. Several key conclusions can be drawn from this map. Intuitively, continuous lines are formed at lower strains (i.e. lower printing speeds and higher flow rates). Interestingly, the strain level below which the continuous lines can be obtained varies with the Ec value such that this limiting strain is between 2–2.5 for Ec values higher than ~20 with a few notable exceptions at the highest Ec levels. At lower Ec values, the limiting strain reduces almost linearly with reducing Ec value. The red dashed lines were added to highlight the apparent region in the ε -Ec plane within which continuous prints were obtained.

As mentioned above, inclusion of EGaIn fillers increases the Ec^* of the inks, leading to a higher Ec value for constant standoff height during printing. To capture that effect and its influence of the line continuity, Fig. S5 in the supporting information separates the same results into plots corresponding to each material. These plots demonstrate that the general continuity of the lines increases with the increasing EGaIn content in the inks. It can be concluded that the increased Ec^* (through increased relaxation time and reduced viscosity) induced by the high EGaIn particle and/or low graphene content enables printability at lower flow rates and higher printing speeds (i.e. higher strains) and higher stand-off distances. In the rheological context, the elastocapillary number represents the relative strength of the elastic effects with respect to the viscous effects in a given liquid (Mckinley, 2005). Considering the results regarding elastocapillary lengths of different ink compositions, one could conclude that EGaIn fillers thus "strengthen" the elastic effects which promotes a deposition mechanism where a stable ink filament is stretched between the nozzle and the substrate, whereas the graphene fillers generally induce an inverse effect. This result is consistent with our earlier findings involving EGaIn and Graphene only composite inks (Nesaei et al., 2019). As these elastic effects weaken, viscous effects promote a mechanism where the ink that exits the nozzle form droplets rather than continuous filaments in tension leading to B-type line formation, particularly observed at high standoff distances. The distinct influence of the EGaIn fillers towards printability at high strains can be observed through the two specific data points circled in Fig. 6(c) indicating continuous prints at strain levels over 2. These two data points belong to the EG2.5 formulation and under the same conditions the control ink G2.5 failed to achieve continuous prints.

Printed filaments forming continuous lines at strains higher than 1 (i.e. under-extrusion condition) are expected to undergo visco-capillary thinning which reduces the lateral line width. Fig. 6(d) presents the width of the lines, measured through optical profilometry. The linewidths measured around the strain of 1 (i.e. balanced extrusion) can be observed to be larger than the nozzle diameter of 200 μm. This result can be explained by the spreading of the inks after their deposition on the glass substrates. It should be noted that these width measurements were taken after spreading of the ink on the glass substrates and drying of the ink solvent. Considering that the solvent constitutes 70 % of the ink volume, considerable spreading of the inks following the deposition is expected.

At low strain levels, the linewidths at the highest Ec value, corresponding to the ink EG2.5 are larger compared to the two other cases. High amount of spreading of EG2.5 can be linked to its low shear viscosity and high density (due to the high density of EGaIn), given that the gravitational effects are a critical contributor in ink spreading (Friedrich and Begley, 2020). This postulation is somewhat contradicted by the fact that the spreading of G2.5 (Ec = 34.97) is higher than E2G3 (Ec = 49.44) despite its higher viscosity and lower density. This discrepancy can possibly be explained by (1) slightly lower value of the exact strain recorded for G2.5, indicating that the actual measured flow rate is

slightly higher compared to the other two cases and (2) possible contact line pinning effects induced by the higher graphene concentration suppressing the spreading behavior (Fukai et al., 2006). Nevertheless, at higher strains, line widths of these three materials are closer to one another as the capillary effects due to solvent's surface tension starts to dominate the inertial flow effects. Among these cases, only EG2.5 with the highest Ec value can "survive" strains over 2 for which the linewidths as small as 100 μm can be obtained. These results reveal that increased ink elasticity induced by the EGaIn fillers in these composites enable lateral printing resolution that is smaller than the nozzle diameters.

3.3. Electrical conductivity

The electrical conductivities of the lines printed using different inks at the lowest tested strain and stand-off distance levels are presented in Fig. 7(a). Under these conditions, the inks are deposited near the balanced extrusion regime thus the measured conductivity values are isolated from the effects coming from ink filament deformation outside the nozzle. From this plot, it could be inferred that graphene fillers are the main contributors to the conductivity. To understand the influence of EGaIn on the composite conductivity, one can compare the conductivity of EG2.5 and E1G4 with their corresponding control inks G2.5 and G4, respectively. As such, EG2.5 exhibit significantly higher electrical conductivity than G2.5 whereas E1G4 and G4 inks exhibit nearly the same conductivity.

These results indicate that EGaIn fillers increase the electrical conductivity of the composite, particularly at high EGaIn filler concentrations. Further analysis involving a large set and variety of inks is necessary to robustly assess and quantify this contribution. It should be noted that this is not a trivial finding. As indicated by several studies cited in the introduction, the oxide skin encapsulating such particles are known to prevent them forming conductive connections. Accordingly, it can be preliminarily concluded that the contribution of the EGaIn fillers to conductivity is a function of the other conductive fillers in the composite.

To understand how this contribution vary with strain, Fig. 7(b) compares the variation of electrical conductivity of EG2.5 and G2.5 lines as a function of printing strain. As shown, the conductivity of EG2.5 lines reduce with increasing strain values, unlike G2.5 in a similar strain range. To see if this behavior holds throughout out the tested ink compositions, we calculated normalized conductivity values for each printed line by dividing the line conductivity with the average conductivity of all the continuous lines from the same material and plotted the results as a function of strain in Fig. 7(c), separately for inks that include and exclude EGaIn fillers. This normalization enables comparison of inks with varying graphene content by removing the inherent material conductivity differences. As indicated by the linear regression lines, presence of EGaIn fillers generally induce a strain dependent conductivity behavior in the printed structures.

To understand the mechanism behind this behavior, we examined the scanning electron microscope images of the printed lines, focusing on the EG2.5 inks. We observed the morphology of the ink constituents on the surface of the printed lines. We focused on two regions: center of the lines where target printing speed and, thus strain is in effect (Fig. 8(a)) and at the end points where the printing speed is down to zero, thus no strain is present (Fig. 8(b)). As shown, EGaIn fillers that are normally circular under zero strain, tend to take elliptical shapes under positive strains, with their major axes aligned along the printing direction. To analyze this quantitatively, we used image processing (ImageJ software) to measure particle dimensions parallel (W) and perpendicular (H) to the printing direction for several experiments as illustrated in Fig. 8(c). To this end, we considered three experiments with varying strain levels, calculated the average H/W ratio corresponding to 15 particles extracted from both the center and end points of the printed lines, and plotted the difference between these ratios corresponding to the center and end points and presented in Fig. 8(d). Here, smaller H/W ratio indicates a larger particle deformation from circular shape (for which $H/W = 1$). The line end points where no strain is present, is used a reference for each experiment through the ratio difference calculation. As shown, the ratio difference increases with increasing strain, indicating increasing stretching of the EGaIn particles along the printing direction. The individual H/W ratios for the end and center points of the lines studied in this analysis is provided in the supporting information, Fig. S8.

This deformation is expected due to the liquid phase cores of these filler particles at this particular size scale (Lear et al., 2017). Furthermore, such a deformation will increase the electrical resistance of an isolated particle. Given that the EGaIn fillers contribute to the bulk conductivity, it can be postulated that the conduction through these fillers is a part of the electrical conduction mechanism of these composites. Accordingly, increase in the resistance of the particles yields a reduction in the bulk conductivity of the composite as observed in Fig. 7(c). It should be noted that a secondary mechanism through which increasing printing strain reduces electrical conductivity would be the stretching of the binder phase and the associated separation of the conductive graphene flakes. In fact, presence of such an effect is evident from the slight strain-dependent reduction of the conductivity of the non-EGaIn containing inks in Fig. 7(c). However, substantially higher rate at which the conductivity of EGaIn containing inks reduce with printing strain indicates that the filler particle deformation is likely the dominant mechanism of conductivity variation in these inks.

4. Conclusions and outlook

Presented results demonstrate that liquid metal fillers introduce viscoelasticity to graphene-PEO composites inks, which substantially improve the processability of this material system, specifically through direct-ink-writing. Particularly, inks including EGaIn fillers could be printed at combinations of higher speeds, lower flow rates and higher standoff distances, allowing more robust, higher throughput application of additive manufacturing in processing of PCs. The capability of EGaIn

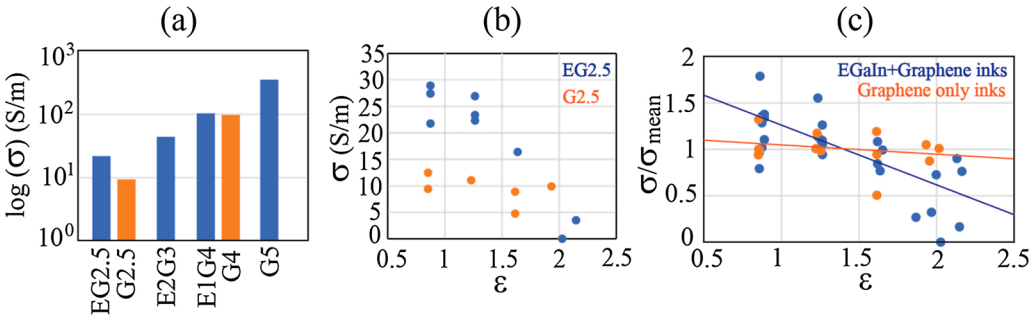

Fig. 7. Results of the electrical conductivity characterization; (a) Conductivity of each tested material, obtained near balanced extrusion with the lowest standoff distance, (b) Strain-dependent variation of electrical conductivity of EG2.5 and G2.5, (c) Strain-dependent variation of normalized electrical conductivity for composites with EGaIn-Graphene and only Graphene fillers.

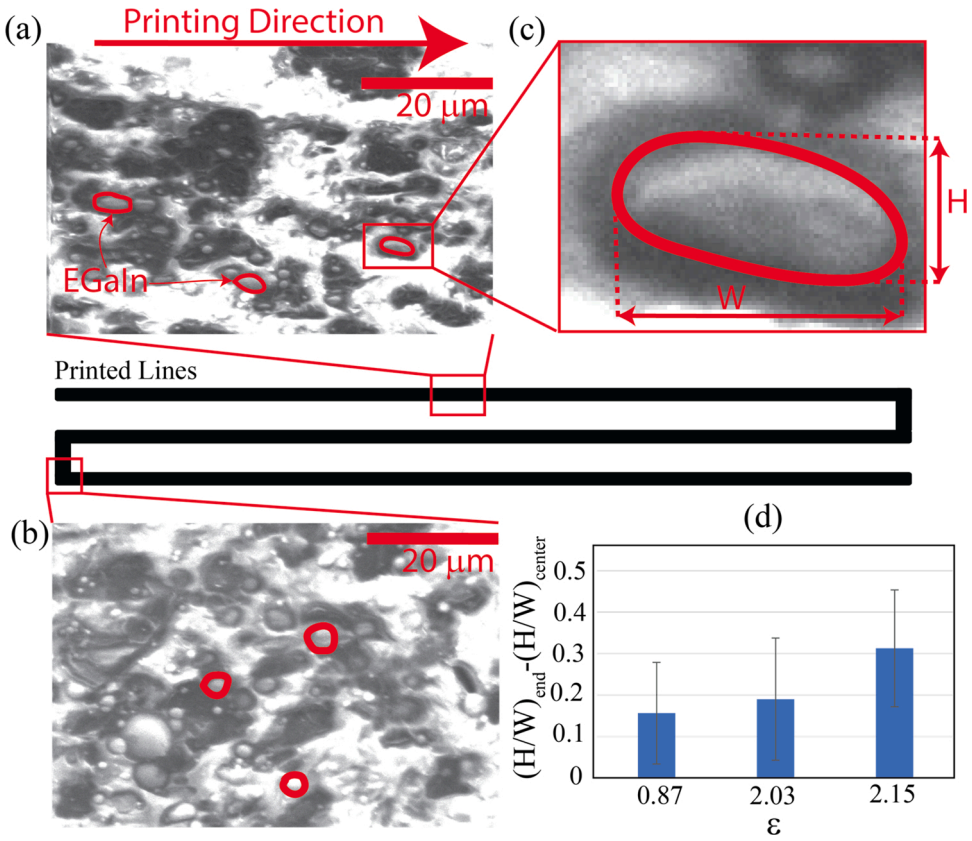

Fig. 8. SEM characterization of the EG2.5 lines; (a) SEM image obtained from the line center, (b) SEM image obtained from the line end, (c) Details of the width and height measurement of the EGaIn particles, (d) H/W ratio difference as a function of printing strain.

including inks to withstand high extensional strains and associated viscoelastic thinning enables printing of filaments that are substantially smaller than nozzle diameter, increasing the process resolution. Regarding electrical properties, we have obtained preliminary evidence that EGaIn fillers also increase the inherent conductivity of the graphene-PEO composites. More importantly, the electrical conductivity of the EGaIn including composites is a strong function of printing process parameters, enabling spatial control of the conductivity in 3D printed composites through variation of process parameters such as speed and flow rate. These findings indicate that PCs including EGaIn fillers carry a great potential to advance the applications utilizing conductive PCs, particularly emerging technologies that are powered by the unique capabilities of additive manufacturing and can benefit from precise control of electrical conductivity. These applications include flexible-stretchable electronics (Muth et al., 2014), biochemical sensors (Nesaei et al., 2018) and printable energy devices (Sun et al., 2013a).

Future research outlook includes several key directions: One of these directions is a detailed study of the influence of EGaIn fillers on the mechanical properties of the complex 3D printed structures of graphene composites. Secondly, inks with higher graphene content should be investigated. Such inks are known to exhibit high viscosities and yield stresses dominated by particle networks of graphene, rendering them difficult to process through direct-ink-writing (Majesté, 2016). EGaIn fillers and the associated viscoelasticity induced in the ink rheology can potentially increase the processability of such inks by reducing shear viscosity and yield stress, allowing shear and extensional flow induced alignment of graphene fillers at higher graphene concentrations, that would normally be hindered by plug flow effects (Siqueira et al., 2017), realizing composites with unprecedent levels of electrical conductivity. Finally, combination of EGaIn fillers with other carbonous (e.g. graphite, carbon nanotubes etc.) or metallic (i.e. silver, gold nanoparticles) fillers as well as different polymer binders should be explored.

Data availability

No data was used for the research described in the article.
Data will be made available on request.
The data that has been used is confidential.

Funding statement

This work was financially supported by the National Science Foundation (NSF) grant 1846758.

CRediT authorship contribution statement

Ruchira Tandel: Methodology, Formal analysis, Investigation, Data curation, Writing - original draft, Writing - review & editing, Visualization. **B. Arda Gozen:** Conceptualization, Methodology, Software, Formal analysis, Data curation, Writing - original draft, Writing - review & editing, Visualization, Supervision, Project administration, Funding acquisition.

Declaration of Competing Interest

The authors declare they have no conflict of interest.

Acknowledgements

Authors would like to acknowledge Sam Karcher for his help with scanning electron microscopy.

Appendix A. Supplementary data

Supplementary material related to this article can be found, in the

online version, at doi:https://doi.org/10.1016/j.jmatprotec.2021.117470.

References

Anna, S.L., McKinley, G.H., 2001. Elasto-capillary thinning and breakup of model elastic liquids. J. Rheol. (N. Y. N. Y). 45, 115. https://doi.org/10.1122/1.1332389.

Bartlett, M.D., Kazem, N., Powell-palm, M.J., Huang, X., Sun, W., 2017. High Thermal Conductivity in Soft Elastomers with Elongated Liquid Metal Inclusions, pp. 3–8. https://doi.org/10.1073/pnas.1616377114.

Boley, J.W., White, E.L., Chiu, G.T.-C., Kramer, R.K., 2014. Direct writing of gallium-indium alloy for stretchable electronics. Adv. Funct. Mater. 24, 3501–3507. https://doi.org/10.1002/adfm.201303220.

Boley, J.W., White, E.L., Kramer, R.K., 2015. Mechanically sintered gallium-indium nanoparticles. Adv. Mater. 27, 2355–2360. https://doi.org/10.1002/adma.201404790.

Chatterjee, T., Krishnamoorti, R., 2013. Rheology of polymer carbon nanotubes composites. Soft Matter. https://doi.org/10.1039/c3sm51444g.

Chiechi, R.C., Weiss, E.A., Dickey, M.D., Whitesides, G.M., 2008. Eutectic gallium–indium (EGaIn): a moldable liquid metal for electrical characterization of self-assembled monolayers. Angew. Chem. 120, 148–150. https://doi.org/10.1002/ange.200703642.

Clasen, C., Phillips, P.M., Palangetic, L., Vermant, J., 2012. Dispensing of Rheologically Complex Fluids. The Map of Misery 58. https://doi.org/10.1002/aic.

Dababneh, A.B., Ozbolat, I.T., 2014. Bioprinting technology: a current state-of-the-Art review. J. Manuf. Sci. Eng. Trans. ASME 136. https://doi.org/10.1115/1.4028512.

Donnet, J., Vidal, A., 1986. Carbon black: surface properties and interactions with elastomers. Adv. Polym. Sci. 76, 103–127.

Elliott, A.M., Ivanova, O.S., Williams, C.B., Campbell, T.A., 2012. An investigation of the effects of quantum dot nanoparticles on photopolymer resin for use in polyjet direct 3D printing. 23rd Annu. Int. Solid Free. Fabr. Symp. - An Addit. Manuf. Conf. SFF 2012 988–998.

Friedrich, L., Begley, M., 2020. Changes in filament microstructures during direct ink writing with a yield stress fluid support. ACS Appl. Polym. Mater. 2, 2528–2540. https://doi.org/10.1021/acsapm.0c00126.

Fukai, J., Ishizuka, H., Sakai, Y., Kaneda, M., Morita, M., Takahara, A., 2006. Effects of droplet size and solute concentration on drying process of polymer solution droplets deposited on homogeneous surfaces. Int. J. Heat Mass Transf. 49, 3561–3567. https://doi.org/10.1016/j.ijheatmasstransfer.2006.02.049.

Guo, R., Cui, B., Zhao, X., Duan, M., Sun, X., Zhao, R., Sheng, L., Liu, J., Lu, J., 2020. Cu-EGaIn enabled stretchable e-skin for interactive electronics and CT assistant localization. Mater. Horizons 7, 1845–1853. https://doi.org/10.1039/c9mh02066g.

Harrison, H.B., 1989. Obtaining specific contact resistance from transmission line model measurements. IEEE Trans. Energy Convers. 4, 160–165. https://doi.org/10.1109/60.17906.

Jakus, A.E., Secor, E.B., Rutz, A.L., Jordan, S.W., Hersam, M.C., Shah, R.N., 2015. Three-dimensional printing of high-content graphene scaffolds for electronic and biomedical applications. ACS Nano 9, 4636–4648. https://doi.org/10.1021/acsnano.5b01179.

Kazem, N., Bartlett, M.D., Majidi, C., 2018. Extreme toughening of Soft materials with liquid metal. Adv. Mater. 1706594. https://doi.org/10.1002/adma.201706594, 1706594.

Lear, T.R., Hyun, S.H., Boley, J.W., White, E.L., Thompson, D.H., Kramer, R.K., 2017. Liquid metal particle popping: macroscale to nanoscale. Extrem. Mech. Lett. 13, 126–134. https://doi.org/10.1016/j.eml.2017.02.009.

Li, Y.Y., Li, L.T., Li, B., 2015. Direct ink writing of 3-3 piezoelectric composite. J. Alloys. Compd. 620, 125–128. https://doi.org/10.1016/j.jallcom.2014.09.124.

Lipatov, Y.S., Feinerman, A.E., 1971. The concentration dependence of surface tension of polymer solutions. J. Adhes. 3, 3–12. https://doi.org/10.1080/00218467108075001.

Majesté, J.C., 2016. Rheology and processing of polymer nanocomposites: theory, practice, and New challenges. Rheology and Processing of Polymer Nanocomposites, pp. 69–134. https://doi.org/10.1002/9781118969809.ch3.

Mckinley, G.H., 2005. Visco-elasto-Capillary thinning and break-up of complex fluids. Rheol. Rev. 2005, 1–48. https://doi.org/10.1007/s00247-009-1482-4.

Muth, J.T., Vogt, D.M., Truby, R.L., Mengüç, Y., Kolesky, D.B., Wood, R.J., Lewis, Ja., 2014. Embedded 3D printing of strain sensors within highly stretchable elastomers. Adv. Mater. 26, 6307–6631. https://doi.org/10.1002/adma.201400334.

Nesaei, S., Rock, M.D., Wang, Y., Kessler, M., Gozen, A., 2017. Additive manufacturing with conductive, viscoelastic polymer composites: direct-ink-Writing of electrolytic and anodic poly(ethylene oxide) composites. J. Manuf. Sci. Eng. Addit. 139, 1–52. https://doi.org/10.1115/1.4037238.

Nesaei, S., Song, Y., Wang, Y., Ruan, X., Gozen, A., Lin, Y., 2018. Micro additive manufacturing of glucose biosensors: a feasibility study. Anal. Chim. Acta. https://doi.org/10.1016/j.aca.2018.09.012.

Nesaei, S., Cavanagh, D.J., Gozen, A., 2019. Rheology of liquid metal particle-based polymer composites: a comparative study. J. Rheol. 63, 559–568. https://doi.org/10.1122/1.5082662.

Neumann, T.V., Facchine, E.G., Leonardo, B., Khan, S., Dickey, M.D., 2020. Direct write printing of a self-encapsulating liquid metal-silicone composite. Soft Matter 16, 6608–6618. https://doi.org/10.1039/d0sm00803f.

Nimmakayala, M., Raju, V.R.K., 2015. Numerical simulation of rod-climbing effect in newtonian fluids. Procedia Eng. 127, 405–412. https://doi.org/10.1016/j.proeng.2015.11.388.

Rošic, R., Pelipenko, J., Kocbek, P., Baumgartner, S., Bešter-Rogač, M., Kristl, J., 2012. The role of rheology of polymer solutions in predicting nanofiber formation by electrospinning. Eur. Polym. J. 48, 1374–1384. https://doi.org/10.1016/j.eurpolymj.2012.05.001.

Sargolzaeiaval, Y., Ramesh, V.P., Neumann, T.V., Miles, R., Dickey, M.D., Öztürk, M.C., 2019. High thermal conductivity silicone elastomer doped with graphene nanoplatelets and eutectic GaIn liquid metal alloy. ECS J. Solid State Sci. Technol. 8, P357–P362. https://doi.org/10.1149/2.0271906jss.

Seah, T.H., Pumera, M., 2011. Platelet graphite nanofibers/soft polymer composites for electrochemical sensing and biosensing. Sens. Actuators, B Chem. 156, 79–83. https://doi.org/10.1016/j.snb.2011.03.075.

Siqueira, G., Kokkinis, D., Libanori, R., Hausmann, M.K., Gladman, A.S., Neels, A., Tingaut, P., Zimmermann, T., Lewis, J.A., Studart, A.R.A.R., 2017. Cellulose nanocrystal inks for 3D printing of textured cellular architectures. Adv. Funct. Mater. 27, 1–10. https://doi.org/10.1002/adfm.201604619.

Skylar-Scott, M.A., Gunasekaran, S., Lewis, J.A., 2016. Laser-assisted Direct Ink Writing of Planar and 3D Metal Architectures, pp. 1–6. https://doi.org/10.1073/pnas.1525131113.

Spiegelberg, S.H., Ables, D.C., McKinley, G.H., 1996. The role of end-effects on measurements of extensional viscosity in filament stretching rheometers. J. Nonnewton. Fluid Mech. 64, 229–267. https://doi.org/10.1016/0377-0257(96)01439-5.

Sun, K., Wei, T.-S., Ahn, B.Y., Seo, J.Y., Dillon, S.J., Lewis, J.a, 2013a. 3D printing of interdigitated Li-ion microbattery architectures. Adv. Mater. 25, 4539–4543. https://doi.org/10.1002/adma.201301036.

Sun, X., Sun, H., Li, H., Peng, H., 2013b. Developing polymer composite materials: Carbon nanotubes or graphene? Adv. Mater. 25, 5153–5176. https://doi.org/10.1002/adma.201301926.

Tutika, R., Zhou, S.H., Napolitano, R.E., Bartlett, M.D., 2018. Mechanical and functional tradeoffs in multiphase liquid metal, solid particle Soft composites. Adv. Funct. Mater. 28, 1–13. https://doi.org/10.1002/adfm.201804336.

Wang, Z., Smith, D., 2018. Rheology effects on predicted Fiber orientation and elastic properties in large scale polymer composite additive manufacturing. J. Compos. Sci. 2, 10. https://doi.org/10.3390/jcs2010010.

Wang, J., Cai, G., Li, S., Gao, D., Xiong, J., Lee, P.S., 2018. Printable superelastic conductors with extreme stretchability and robust cycling endurance enabled by liquid-metal particles. Adv. Mater. 1706157. https://doi.org/10.1002/adma.201706157, 1706157.

Wei, M., Zhang, F., Wang, W., Alexandridis, P., Zhou, C., Wu, G., 2017. 3D direct writing fabrication of electrodes for electrochemical storage devices. J. Power Sources 354, 134–147. https://doi.org/10.1016/j.jpowsour.2017.04.042.

Yuk, H., Zhao, X., 2018. A new 3D printing strategy by harnessing deformation, instability, and fracture of viscoelastic inks. Adv. Mater. 30, 1–8. https://doi.org/10.1002/adma.201704028.

Yun, G., Tang, S.Y., Zhao, Q., Zhang, Y., Lu, H., Yuan, D., Sun, S., Deng, L., Dickey, M.D., Li, W., 2020. Liquid metal composites with Anisotropic and unconventional piezoconductivity. Matter 3, 824–841. https://doi.org/10.1016/j.matt.2020.05.022.

Zhao, J., Morgan, A.B., Harris, J.D., 2005. Rheological characterization of polystyrene-clay nanocomposites to compare the degree of exfoliation and dispersion. Polymer (Guildf). 46, 8641–8660. https://doi.org/10.1016/j.polymer.2005.04.038.

Zhu, S., So, J.-H., Mays, R., Desai, S., Barnes, W.R., Pourdeyhimi, B., Dickey, M.D., 2013. Ultrastretchable fibers with metallic conductivity using a liquid metal alloy core. Adv. Funct. Mater. 23, 2308–2314. https://doi.org/10.1002/adfm.201202405.